https://doi.org/10.5194/esd-2022-28
Preprint. Discussion started: 22 August 2022

Earth System Dynamics
Discussions

How does the phytoplankton-light feedback affect marine N2O inventory?

Sarah Berthet [1*], Julien Jouanno [2], Roland Séférian [1], Marion Gehlen [3], William Llovel [4]
[1] CNRM, Université de Toulouse, Météo-France, CNRS, Toulouse, France
[2] LEGOS, Université de Toulouse, IRD, CNRS, CNES, UPS, Toulouse, France
[3] LSCE, Institut Pierre Simon Laplace, Gif-Sur-Yvette, France
[4] LOPS, CNRS/University of Brest/IFREMER/IRD, Brest, France

([*]correspondence: sarah.berthet@meteo.fr)

Abstract

The phytoplankton-light feedback (PLF) depicts how phytoplankton biomass interacts with the downwelling shortwave radiation entering the ocean. Considering the PLF allows differential heating across the ocean water column as a function of the phytoplankton concentration. Only one third of the CMIP6 Earth system models include a complete representation of the PLF. In other models, the PLF is mimicked either thanks to a prescribed climatology of chlorophyll or not represented at all. Consequences of an incomplete representation of the PLF on the marine biogeochemical content haven't been assessed yet and remain a source of multi-model uncertainty in future projection. Here, we scrutinize with a single modelling set-up how various representation of the PLF can impact ocean physics and ultimately marine production of a major greenhouse gas, the nitrous oxide (N2O). Global sensitivity experiments considering the ocean, sea ice and marine biogeochemistry have been performed at 1-degree of horizontal resolution over the last two decades (1999-2018). We show that the representation of the PLF has significant consequences on the ocean heat uptake and temperature of the first 300 meters of the tropical ocean. Temperature anomalies due to an incomplete PLF representation drive perturbations of the ocean stratification, dynamics and oxygen concentration. Different projection pathways for N2O production result from the choice of the PLF representation. Considering an incomplete representation of the PLF overestimates the oxygen concentration in the North-Pacific oxygen minimum zone and underestimates the local N2O production. This leads to important regional differences of sea-to-air N2O fluxes: fluxes are enhanced by up to 24% in the south Pacific and south Atlantic subtropical gyres, but reduced by up to 12% in oxygen minimum zones of the northern hemisphere. Our results based on a global ocean-biogeochemical model at CMIP6 state-of-the-art thus shine a light on a current uncertainty of the modelled marine nitrous oxide budget in that climate models.

Plain language summary

Phytoplankton absorbs the solar radiation entering the ocean surface, and contributes to keep the associated energy in surface waters. This natural effect is not commonly represented in the oceanic part of climate models, or often suffers simplifications. We show that an incomplete representation of this biophysical interaction affects the way climate models capture ocean warming, what in turn uncertains the forecast of oceanic emissions of an important greenhouse gas called the nitrous oxide.

Key-words: phytoplankton-light interaction; bio-physical feedback; nitrous oxide; N2O; CMIP6 Earth system models; CNRM-ESM2-1; ocean-biogeochemical model; greenhouse gazes; marine emission; climate

https://doi.org/10.5194/esd-2022-28
Preprint. Discussion started: 22 August 2022

Earth System Dynamics Discussions

Key points:

- forced ocean-biogeochemical experiments reveal that marine production of nitrous oxide is sensitive to the representation of the phytoplankton-light feedback
- the phytoplankton-light feedback perturbs the accumulation of heat and the ocean dynamics which drive changes in nitrous oxide production patterns
- an incomplete phytoplankton-light feedback overestimates sea-to-air N2O fluxes by up to 24% in subtropical gyres and reduces them by up to 12% in oxygen minimum zones

1. Introduction

Couplings between the physical, biogeochemical, or ecosystem compartments of the ocean can induce abrupt system changes (Heinze et al., 2021). Currently, the only coupling in Earth system models existing between modelled marine biogeochemistry and ocean dynamics is the interactive phytoplankton-light feedback (PLF) (Séférian et al., 2020). It is at play when the chlorophyll (CHL) produced by the biogeochemical compartment is used to determine the fraction of shortwave radiation (SW) penetrating into the ocean surface waters. In this case, the CHL concentration mimicking the influence of the marine biota on the vertical redistribution of heat in the upper ocean is consistent (because the same) with the one used to compute biogeochemical cyclings.

a) Phytoplankton-light feedback (PLF)

Since the first observational evidences on how surface materials may impact light absorption by the ocean and change the radiative imbalance within the mixed-layer depth (Kahru et al. 1993), several ocean models have gradually accounted for this biophysical interaction. Gildor and Naik (2005) highlighted the importance to consider monthly variations of CHL to capture the first-order effect of marine biota on light penetration in ocean models. Then, introducing a light-interactive CHL in numerical experiments has been shown to affect oceanic phenomenons on a wide range of spatial and temporal scales. Enabling a phytoplankton-light interaction modifies the intensity of the spring-bloom in subpolar regions (Oschlies, 2004), the maintenance of the Pacific Cold Tongue (Anderson et al., 2007), the seasonality of the Arctic Ocean (Lengaigne et al., 2009), the strength of the tropical Pacific annual cycle and the ENSO variability (Timmermann and Jin, 2002; Marzeion et al., 2005), the northward extension of the meridional overturning circulation (Patara et al., 2012), and the cooling of the Atlantic and Peru-Chili upwelling systems (Hernandez et al., 2017, Echevin et al., 2022).

However the mean effect of the PLF on sea surface temperature (SST) has been argued to depend on the numerical framework (forced ocean versus coupled ocean-atmosphere models). The conflicting results obtained on that topic in the literature have been shown to be mainly due to diverging bio-optical protocols among models rather than by the inclusion of air-sea coupling. Following Park et al. (2014) the atmosphere-ocean coupling just acts to amplify the PLF-induced mean change, but does not alter the sign of the response obtained in ocean-only experiments. Two main causal chains have been proposed to interpret the sign of the final heat perturbation, opposing the proeminence of an indirect dynamical response (Murtugudde et al., 2002; Löptien et al., 2009) to that of a direct thermal effect (Mignot et al., 2013; Hernandez et al., 2017). Regional dependencies of these two mechanisms have also been evidenced (Park et

https://doi.org/10.5194/esd-2022-28
Preprint. Discussion started: 22 August 2022

al., 2014). However, beyond the diversity of model responses, a consensus emerges about the first order effect the PLF exerts on the ocean, being to perturb the ocean thermal structure (Nakamoto et al., 2001; Murtuggude et al., 2002; Oschlies, 2004; Manizza et al., 2005, 2008; Anderson et al., 2007; Lengaigne et al., 2007; Gnanadesikan and Anderson, 2009; Löptien et al., 2009; Patara et al., 2012; Mignot et al., 2013; Hernandez et al., 2017). By trapping more heat at the ocean surface in eutrophic regions, such as coastal or equatorial upwellings areas, the presence of phytoplankton increases the surface warming. Confining heat at the surface leads to less heat penetrating into the ocean interior. Because these effects depend on upper ocean stratification, they are more active during local summer and at low latitudes. An important role is attributed to modelled seasonal deepening of the mixed layer as it determines the intensity of the underlying temperature anomaly and its vertical movement to the surface. In other terms, whatever the temporality of the causal chain, changes in the PLF representation are expected to both pertub the ocean heat uptake, and trigger perturbations of both the water column stratification and associated ocean dynamics.

b) This study: implications for N2O budget uncertainties

Nitrous oxide (N2O) is a major ozone-depleting substance (Ravishankara et al., 2009; Freing et al., 2012) and a potent greenhouse gas, whose global warming potential is 265-298 times that of CO2 for a 100-year timescale (Myhre et al., 2013). The spatial coincidence between marine productive areas and observed hot-spots of N2O production leads to question the impact of an incomplete representation of the PLF on the simulated N2O inventory. Indeed recent observational studies highlight that N2O production is high in low-oxygen tropical regions and cold upwelling waters (Arévalo-Martinez et al 2018; 2020; Yang et al., 2020; Wilson et al., 2020). N2O has been shown to become more highly saturated in the surface waters of equatorial upwelling regions due to the upward advection of N2O-rich waters (Arévalo-Martínez et al., 2017). Thus, regions known to account for the most productive areas of the ocean spatially coincide with the highest N2O production: 64% of the annual N2O flux occurs in the tropics, and 20% in coastal upwelling systems that occupy less than 3% of the ocean area (Yang et al., 2020).

Despite these recent results, a large range of uncertainties still surrounds oceanic N2O emissions, as large areas of both the open and coastal ocean remain undersampled by observations (Wilson et al., 2020). In particular, the sparcity of observational data in regions which emit considerable amounts of this gas contributes to increase the uncertainties. The recent global budget of Tian et al. (2020) estimates natural sources from soils and oceans contributing up to 57% to the total N2O emissions for the recent decade, with the ocean flux reaching 3.4 (2.5−4.3) Tg N yr^{-1}. But this oceanic contribution reflects a large uncertainty range, as it has been computed based on global ocean-biogeochemical models (and moreover based on a very small number of models). Indeed very few climate models, even in the current CMIP6 generation, include emissions (and beforehand a complete representation of N cycling) of N2O fluxes: only 4 out of the 26 Earth system models considered in Séférian et al. (2020) model marine N2O emissions.

Finally, this last generation of Earth system models projects an enhanced ocean warming in response to climate change, which is in turn expected to increase upper-ocean stratification (Sallée et al., 2021) and to contribute to greater reductions in upper-ocean nitrate and

https://doi.org/10.5194/esd-2022-28
Preprint. Discussion started: 22 August 2022

subsurface oxygen ventilation (Kwiatkowski et al., 2020). Ocean warming and deoxygenation constitute two triggers of high-probability high-impact climate tipping points (Heinze et al., 2021), which have been identified as two of the main environmental factors influencing marine nitrous oxide (N2O) distributions (IPCC, 2019; Hutchins and Capone, 2022). Through the addition of its expected imprints on the upper ocean stratification, the PLF representation could further change the oceanic N2O source by modulating the mixing between N2O-rich water and intermediate depths, perturbing the way N2O-rich water reach the air-sea interface (Freing et al., 2012).

In that perspective, the present study investigates how an incomplete representation of the phytoplankton-light feedback may particularly uncertain nitrous oxide prediction in an up-to-date global ocean-biogeochemical model making up the current generation of Earth system models. Section 2 describes the numerical model and the set of experiments encompassing the existing options to consider CHL modulations of the incoming SW radiation. The N2O parametrization used in this model is also detailled. Section 3 presents the important effect of an interactive PLF on the ocean heat content, associated ocean stratification and dynamics, and its repercussions on marine N2O inventory. Finally, Section 4 summarizes the main results, addresses their broader implications, and discusses the future work motivated by this study.

2. Methodology

a) Sensitivity experiments with a global ocean-biogeochemical model

Recent projections of future N2O emissions realized as part of intercomparison projects like CMIP6 are still based on Earth system models with a low spatial resolution (Séférian et al., 2020). For sake of coherence with CMIP biogeochemical modelling efforts, we use a global ocean-biogeochemical configuration of the NEMO-PISCES model (Madec, 2008; Aumont et al., 2015) at 1° of horizontal resolution in the following. This model corresponds to the oceanic component of CNRM-ESM2-1 (Séférian et al., 2019) and is one of the few CMIP6-class models that contributed to the Global N2O budget (Tian et al., 2020). Details on model configuration are given in Berthet et al. (2019). Using an ocean-only configuration allows to isolate the local response induced by the PLF, by not confounding it with potential inter-basin feedbacks acting through the atmosphere.

The global ORCA1 domain was first spun-up under preindustrial conditions during 2000 years by cycling the first 5 years of the JRA55-do atmospheric reanalysis (Tsujino et al., 2018; i.e. OMIP2 compliant: Tsujino et al., 2020). The cycling method was prolonged until year 1958, while considering the historical evolution of atmospheric CO2 and N2O since year 1850. Then the complete period of JRA55-do atmospheric forcing has been rolled out from 1958 to 2018. This first experiment (hereafter chl_inter) together with the spin-up both account for an interactive PLF: the penetration of SW radiation into the ocean surface is constrained by the CHL concentration produced by the PISCES biogeochemical component. Hereafter the term "spin-up" has been extended to the whole period simulated before year 1999.

https://doi.org/10.5194/esd-2022-28
Preprint. Discussion started: 22 August 2022

Earth System Dynamics
Discussions

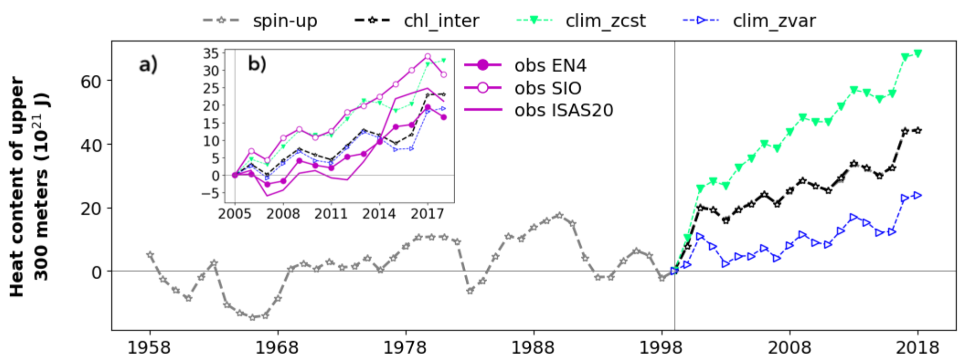

Figure 1: Modelled **tropical [35°S-35°N] heat content of upper 300 m** (OHC300; in ZJ) for each experiment described in Table 1: chl_inter (black; empty stars), clim_zcst (green; full downward triangles) and clim_zvar (blue; empty rightward triangles). In (a) final part of the spin-up has been added in gray to illustrate the branching protocol in year 1999, and OHC300 anomalies have been computed with respect to year 1999. Subplot (b) zooms over the Argo period to compare modelled tropical OHC300 anomalies with 3 in situ-based products (see section 2c).

At year 1999 two other sensitivity experiments were branched off (Figure 1). The experiments clim_zcst and clim_zvar account for an incomplete and external PLF, as they consider an observed climatology of surface CHL from ESACCI (Valente et al., 2016) in order to compute the light penetration into sea water. These two experiments differ from each other by the "realism" of the vertical profile derived from the ESACCI CHL surface climatology (Table 1). The vertical profile used for clim_zcst is considered constant and spreads uniformly in the vertical direction to the level below which we consider the light cannot penetrate (Figure S1, b and d-f). The CHL vertical profile of clim_zvar is variable and derived from the 2D surface climatology following Morel and Berthon (1989) to the level of light extinction (Figure S1, c and d-f). This set of experiments is representative of the several configurations used in the case of CMIP intercomparison project.

Experiment	Which CHL fields to interact with incoming SW radiation?	PLF nature
chl_inter	uses directly the 3D CHL produced by the biogeochemical component	interactive
clim_zcst	uses the prescribed monthly climatology of ESACCI CHL with a constant vertical profile, equal to the value of the surface climatology up to the level of light extinction	incomplete
clim_zvar	uses the prescribed monthly climatology of ESACCI CHL with a variable vertical profile, derived from the surface climatology following Morel and Berthon (1989)	incomplete

Table 1: Experimental set-up.

https://doi.org/10.5194/esd-2022-28
Preprint. Discussion started: 22 August 2022

Note that in clim_zcst and clim_zvar, CHL concentrations used for radiation and biogeochemical cycles are decoupled: the biogeochemical model produces CHL and uses it for biogeochemical element cycling but feedback of CHL on physics (stratification, ocean heat content) is determined by the externally prescribed CHL climatology. In this case the marine biota computed by the biogeochemical model does not affect the physical properties of the ocean waters.

Finally, all three experiments use a simplified formulation of light absorption by the ocean to calculate both the phytoplankton light limitation in PISCES and the oceanic heating rate (Lengaigne et al., 2007). In this formulation, visible light is split into three wavebands: blue (400–500 nm), green (500–600 nm) and red (600–700 nm); for each waveband, the CHL-dependent attenuation coefficient is fitted to the coefficients computed from the full spectral model of Morel (1988) (as modified by Morel and Maritorena (2001)) assuming the same power-law expression.

Consequences on the marine biogeochemical mean state of incomplete representations of the PLF are assessed in the following by difference with our control run chl_inter. This methodology allows to evaluate how different levels of realisms and complexity in resolving bio-physical interactions impact the physical and biogeochemical content of the modelled ocean.

b) N2O parameterization

As described by Aumont et al. (2015), PISCES models five limiting nutrients for phytoplankton growth: nitrate and ammonium, phosphate, silicate and iron. The phosphate, nitrate-ammonium nutrient pools are not really independent in PISCES, as they are linked by a constant and identical Redfield ratio in all the modelled organic compartments. Redfield ratios are set to 122:16:1 for C:N:P following Takahashi et al. (1985) and the -O:C ratio is set to 1.34 (Kortzinger et al., 2001).

In the ocean, N2O production and consumption are driven by marine bacteria in slightly oxygenated waters. N2O can occur as a by-product during microbial nitrification and as an intermediate product during denitrification (Freing et al., 2012). The oxic-anoxic interface above oxygen minimum zones (OMZ) has been shown to provide appropriate conditions to enable N2O production (Ji et al., 2018). In the absence of oxygen, nitrate ($NO3^-$) is the next preferred electron acceptor for respiration after oxygen according to the electrochemical series (Lam and Kuypers, 2011). While nitrification is typically assumed to be an aerobic process, substantial suboxic nitrification has also been reported in many of the world ocean’s major suboxic zones. Denitrification has been shown to be the dominant process for N2O production in the southern (Ji et al., 2015, 2018) and northern (Ji et al., 2018) part of the Pacific OMZ, but uncertainty still subsist: Kalvelage et al. (2013) observe that water-column denitrification was only of minor importance (<<1% total N loss) for the overall N budget in the eastern tropical South Pacific OMZ and that anammox was the dominant mode of N loss at the time of sampling.

The bacterial pool is not yet explicitly modelled in PISCES. Processes of N2O production like nitrification or denitrification are not formally expressed, and PISCES diagnoses their effects from specific environmental conditions. Such modelling approach with an indirect representation of the N2O yield is rather common in present Earth system models due to the

https://doi.org/10.5194/esd-2022-28
Preprint. Discussion started: 22 August 2022

complexity of involved processes (Battaglia and Joos, 2018). For example, in MPI-ESM 1-2-LR (Ilyina et al., 2013) and MIROC-ES2L (Hajima et al., 2020), two of the few other Earth system models simulating marine N2O emissions in CMIP6 (Seferian et al., 2020), the production of N2O is mainly linked to the consumption of oxygen (O2) during remineralization of organic matter.

In PISCES it is assumed that the distribution of nitrifying bacteria in the model is ubiquitous in the ocean interior, so wherever there is export of organic matter to depth the model computes nitrification, consuming ammonium and producing nitrate (Martinez-Rey et al., 2015). Nitrification is particularly enhanced in total absence of light, whereas oxygen levels should be above the suboxic threshold of 1 µmol L^{-1}. Denitrification is computed in the model where dissolved oxygen concentration falls below 5 µmol L^{-1}, which defines suboxic waters (Cocco et al., 2013; Bopp et al., 2013).

In each grid point below 100 m depth (as N2O production is inhibited by light), a unitless function $f(O_2)$ depending on the oxygen concentration $[O_2]$ (in µmol L^{-1}) is computed following:

$$\left.\begin{array}{l} f([O_2] < 1\ \mu mol\ L^{-1}) = [O_2] \\ f(1\ \mu mol\ L^{-1} \leq [O_2] \leq 5\ \mu mol\ L^{-1}) = 1 \\ f([O_2] > 5\ \mu mol\ L^{-1}) = 0.7*\exp(-0.1*([O_2] - 5)) + 0.3*\exp(-0.01*([O_2] - 5)) \end{array}\right\} \quad (1)$$

$f(O_2)$ allows to evaluate the suboxic production of N2O based on Martinez-Rey et al. (2015):

$$[N2O]_{suboxic} = \alpha + \beta * f(O_2) \quad (2)$$

with α being the nitrification coefficient for N2O background production equal to 10^{-4} molN2O per molO_2 consummed. β is the denitrification coefficient which scales the oxygen-dependent function. It is equal to 30 10^{-4} molN2O per molO_2 consummed.
Then the local trend of nitrous oxide concentration [N2O] is finally evaluated by Eq. (3) at each time step as:

$$\begin{array}{lll} d[N2O]/dt = & [N2O]_{suboxic} * zolimit * o2ut & (3.1)\ \text{remineralization} \\ & - sink_{N2O} * [N2O] & (3.2)\ \text{sink term} \\ & + [N2O]_{suboxic} * zonitr * o2nit & (3.3)\ \text{nitrification} \\ & + [N2O]_{suboxic} * zgrazing * o2ut & (3.4)\ \text{grazing} \end{array}$$

where in the first term (3.1) zolimit accounts for ammonification in oxic waters through oxygen consumption during the remineralization of the organic matter at the o2ut ratio of 133/122. In the second term (3.2) $sink_{N2O}$ is the N2O sink term coefficient corresponding to the N2O consummed under anoxic conditions by denitrification at a rate of 7.12 10^{-4} s^{-1}. The third term (3.3) represents the part of N2O concentration produced as an intermediate product of nitrification at a o2nit ratio of 32/122. The last term (3.4) produces N2O by grazing of the remnant organic matter.

The N2O partial pressure difference across the air-sea interface (sea-to-air Dpn2o; in atm) is then computed based on

https://doi.org/10.5194/esd-2022-28
Preprint. Discussion started: 22 August 2022

$$Dpn2o = [N2O]_{surface} / solub_{N2O} - pn2o * P_{atm} \quad (4)$$

with pn2o, the atmospheric partial pressure of N2O equal to 273.021 ppb, P_{atm} the atmospheric pressure in N/m^2, and $solub_{N2O}$ the N2O solubility in mol/m^3 which depends on in-situ temperature and practical salinity following the formulation of Weiss and Price (1980).

Finally sea-to-air N2O fluxes ($mol/m^2/s$) are inferred based on Wanninkhof (1992; 2014):

$$N2O\_flux = Dpn2o * solub_{N2O} * Kg_{N2O} \quad (5)$$

with Kg_{N2O} being the piston velocity for N2O (m/s), which depends on wind speed, ice fraction and temperature .

c) Observations

Model results are compared with available observational-based gridded T/S datasets. Ocean heat content (OHC) of the upper 0-300-meters layer has been inferred from three different products: i) the global objective analysis of subsurface temperature EN4 (Good et al., 2013), ii) the SIO product of the Scripps Institution of Oceanography (Roemmich anf Gilson, 2009), and iii) the ISAS20 optimal interpolation product released by the Ifremer (Kolodziejczyk et al., 2019; Kolodziejczyk et al., 2021). While SIO and ISAS20 products consider only Argo T/S profiles, EN4 dataset considers all types of in situ profiles providing temperature and salinity (when available). These three in situ-based datasets are considered since 2005, when the Argo coverage became sufficient to characterize the global ocean. Details on OHC computation can be found in Llovel and Terray (2016) and Llovel et al. (2022). The text also refers to cross-validations performed on OHC of the deeper layers (0-700 m and 0-2000 m) that have been performed with OHC anomalies from World Ocean Atlas 2009 (Levitus et al., 2012). A monthly climatology (1955-2012) of oceanic temperature from World Ocean Atlas 2013 version 2 (Locarnini et al., 2013) has been used to evaluate modelled temperatures. Modelled O2 has been compared with the annual climatology of O2 from World Ocean Atlas 2013 (Garcia et al., 2014). The recent dataset of Dpn2o observations compiled by Yang et al. (2020) is used to evaluate modelled Dpn2o.

3. Results

a) Impact of PLF on the upper ocean heat content and dynamics

Meridional sections reveal that heat perturbations in response to changing CHL fields interacting with light are limited to the top 0-300 m layer of the ocean and predominantly affect the tropical area (*Figure 2* and Figure S2, c-d).

https://doi.org/10.5194/esd-2022-28
Preprint. Discussion started: 22 August 2022

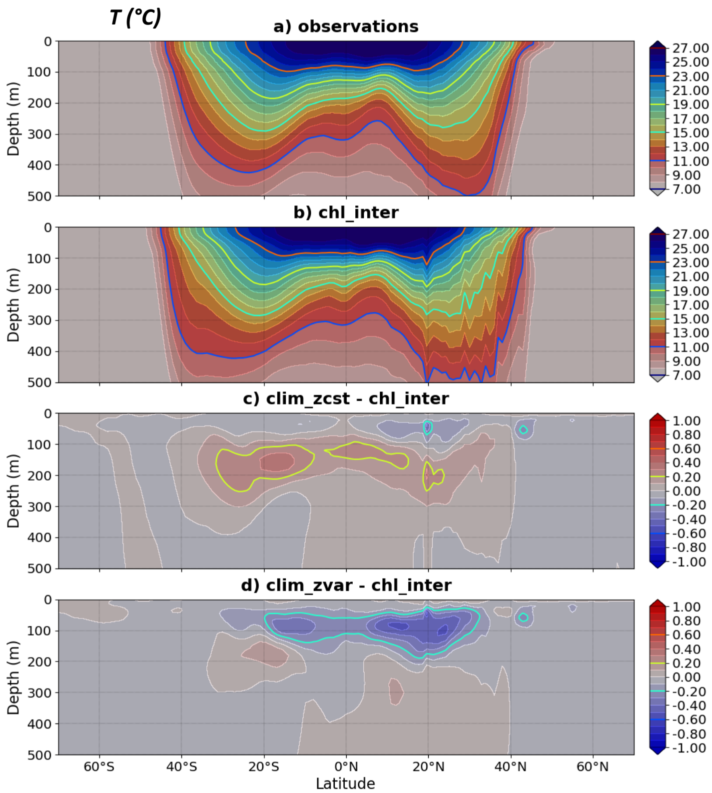

Figure 2: Mean 2009-2018 meridional section of **temperature** (°C) averaged over the whole tropical band (0-360°E) for a) observations, b) chl_inter and its differences with c) clim_zcst and d) clim_zvar.

The largest temperature anomalies are observed near the thermocline depth and reflect upper ocean warming and deepening of the thermocline in clim_zcst (*Figure* 2c), and cooling and shallowing of the thermocline in clim_zvar (*Figure* 2d). In clim_zcst the ocean warming reflects large-scale patterns of a tropical CHL deficit compared to chl_inter (Figure S1, b). Temperature differences seen in the near-surface layer (0-50 m) is lower than that of the 50-300 m layer. This is expected as a result from weak stratification but also from experiments run with a forced atmosphere in which the temperature of the ocean surface layer is constrained by the atmospheric prescribed state.

When using an incomplete representation of the PLF, two contrasting trends of the upper ocean heat content (OHC) emerge compared to our control run chl_inter (Figure 1a).

Over the Argo period (2005-present) EN4 estimates of tropical OHC300 are in very good agreement with our warmest experiment clim_zcst (Figure 1b), while the two other dataproducts SIO and ISAS20 are in better agreement with our control run chl_inter and with clim_zvar. Note that the good accordance between modeled OHC300 and observations is not

https://doi.org/10.5194/esd-2022-28
Preprint. Discussion started: 22 August 2022

Earth System Dynamics
Discussions

to take for granted (Cheng et al., 2016; Liao et al., 2022) and that non-negligible differences among OHC dataproducts exist and are generally particularly strong in the upper 0-300 m layer (Lyman et al., 2010; Liang et al., 2021). The spread between these products at the end of the 2005-2018 period (12.1 10^{21} J) is comparable with that of our numerical set (13.6 10^{21} J). The modelled OHC in chl_inter is in very good agreement with current global mean in situ observations (Meyssignac et al., 2019; see their Figure 11) and with OHC anomalies derived from WOA09 (Levitus et al., 2012). In accordance with these observations, our ocean-biogeochemical model simulates a global mean increase of OHC over the 2006-2016 period of order 40 10^{21} J for the upper 700 m, and of about 70 10^{21} J for the 0-2000 m layer.

Subsurface thermal anomalies develop rapidly (Figure S3) after branching of clim_zvar and clim_zcst in 1999. The dipole structure of the anomaly seen in clim_zcst reflects the surface heat trapping in chl_inter and the associated subsurface cooling (Figure S3, b). Indeed in clim_zcst the vertically constant and weaker profiles of CHL trap less incoming SW than the CHL maximum seen in chl_inter between 0 and 100 m depth (Figure S1, d-f). The negative anomaly in clim_zvar suggests that the parameterization of Morel and Berthon (1989) contributes to underestimate the ocean heat uptake (Figure S3, c and Figure S2, d) by comparison to chl_inter. This heat deficit results from the overestimation of the vertical integral of CHL over large areas of the tropical domain in clim_zvar compared to chl_inter (Figure S1, c), which catch the energy associated to the incoming radiation without distributing it to the water column.

In both clim_zcst and clim_zvar the subsurface temperature anomaly deepens progressively over the first six years of simulation as a result of vertical mixing (Figure S3). This evolution indicates that part of the OHC300 differences between experiments comes from the adjustment of clim_zcst and clim_zvar to the spin-up mean state yielded by an interactive PLF. However, differences in OHC300 from experiments having spin-ups consistent with their own PLF representations are expected to be even greater. The range of uncertainties evaluated here should be considered at the lower end of estimate of OHC discrepancies that may emerge from changing the PLF representation.

Prescribing a constant vertical profile of CHL (clim_zcst; green) to compute the penetration of the radiation into the ocean increases the OHC of the upper 300 meters (hereafter OHC300) by more than 20 10^{21} J during the last two decades (1999-2018) compared to chl_inter (Figure 1). This rise of OHC300 decreases the vertically-weighted sum of the tropical potential density of the upper 300 m at the end of the simulated period by 5 kg/m^3 compared to chl_inter (Figure S4). Surprisingly, the opposite trend (a reduced OHC300 compared to chl_inter) is simulated with the same state-of-the-art CMIP6 ocean-biogeochemical model when considering a variable vertical profile of CHL (clim_zvar; blue). However Figure 1 highlights that the simulation using a consistent CHL for interacting with both incoming SW and biogeochemical cyclings (chl_inter) does not amplify one of these two trends, as clim_zcst and clim_zvar surround chl_inter. Average ranges of uncertainties over the extended tropical domain (35°S-35°N) exceed 40 10^{21} J in terms of OHC300 (Figure 1), 4 meters for the thermocline depth and more than 9 kg/m^3 for the potential density perturbation (Figure S4).

Similar to OHC300, ranges of uncertainty for the OHC estimates of deeper layers (0-700 m and 0-2000 m) also slightly exceed 40 10^{21} J. Such uncertainty ranges are quite important as they have been obtained by only changing the PLF representation in a single ocean-biogeochemical

https://doi.org/10.5194/esd-2022-28
Preprint. Discussion started: 22 August 2022

model. By comparison, in the context of OMIP protocols, Tsujino et al. (2020) give spreads between CMIP models estimates of order 50 10^{21} J for the OHC of the upper 700m after 20 years (see their Figure 24, a-b). Regarding the OHC integrated over the 0-2000m layer, they present an inter-model spread between 50 and 100 10^{21} J, depending on the OMIP protocol considered (see their Figure 24, d-e). So, the OHC300 uncertainty of 40 10^{21} J triggered by the representation of the PLF in our set of experiments has a comparable order of magnitude than the current multi-models estimation of OHC. Part of the OHC multi-model uncertainty in current climate models may be due to different representations of the phytoplankton-light interaction.

The heat and associated density perturbations also cause dynamical modifications of upper ocean currents (Figure *3*). Absolute differences in upper ocean velocities (average between 0 and 300m depth) are between |0.05| and |0.6| cm/s with strongest differences along the equator revealing perturbations of the equatorial undercurrent (Figure *3*, b and c). Circulation around the subtropical gyres is also impacted, in particular for the south-Pacific subtropical gyre. These modifications of zonal and meridional dynamics spread over the entire tropical latitudes, from 30°S to 30°N, strongly supporting the idea that heat perturbations induced by modifying interactions between CHL and incoming SW cause non-negligible modifications of the equatorial and tropical ocean dynamics.

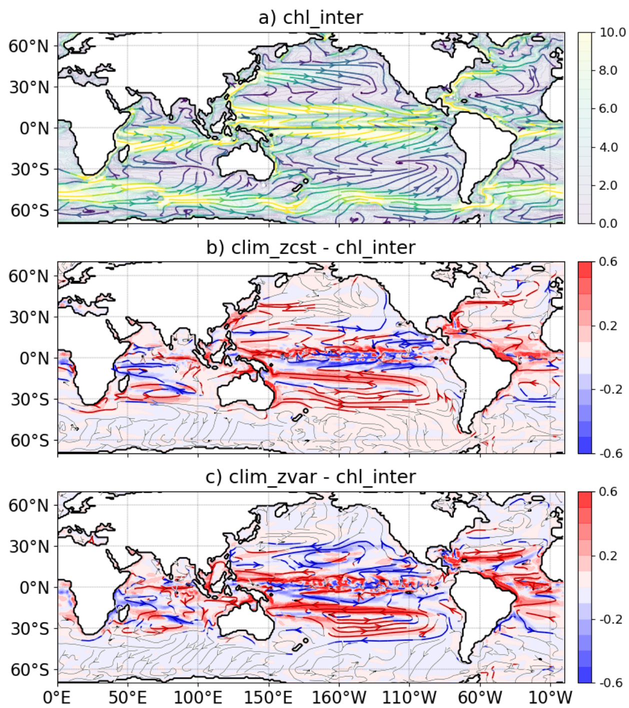

Figure 3: Annual mean speed (color; cm/s) and streamlines of **oceanic currents** between 0-300 m over the 2009-2018 period for a) chl_inter, and its differences with b) clim_zcst and c) clim_zvar. In b-c) streamlines are colored when absolute speed are larger than 0.05 cm/s.

Earth System Dynamics
Discussions

b) PLF impact on N2O production

Perturbations of the annual pycnocline depth (Figure 4, a-c) highlight a vertical adjustment to the large-scale dynamical anomalies (Figure *3*). Variations of the pycnocline integrate perturbations of both thermal and salinity stratifications. However, in our experiments heat anomalies appear to drive perturbations, and pycnocline depth anomalies mainly reflect those of the thermocline. The cold anomaly dominating the tropical domain in clim_zvar (Figure S2, d) appears to be vertically redistributed, as it triggers the raising of the isopycnals (Figure 4, c). In contrast to the anomalies seen over most of the tropical Pacific, a deepening of the isopycnals reaching up to 20 meters is modelled in both South Pacific and Atlantic subtropical gyres in clim_zcst and clim_zvar (Figure 4, b and c). Over these subtropical gyres heat is redistributed along the vertical as the subsurface warm anomaly dives which in turn causes a deepening of the pycnocline (Figure 4, b and c). As stressed by Sweeney et al. (2005), small changes in CHL concentration (Figure S1) may have important effects on the mixed layer depth in these subtropical gyres due to low local wind speeds. Strong winds would drive the mixed layer depth independently of the CHL changes, explaining why the pycnocline is barely perturbed along the equator (Figure 4, b and c). In line with their results, our set of experiments highlights that small CHL changes in low productivity regions trigger a vertical redistribution of density anomalies affecting the stratification.

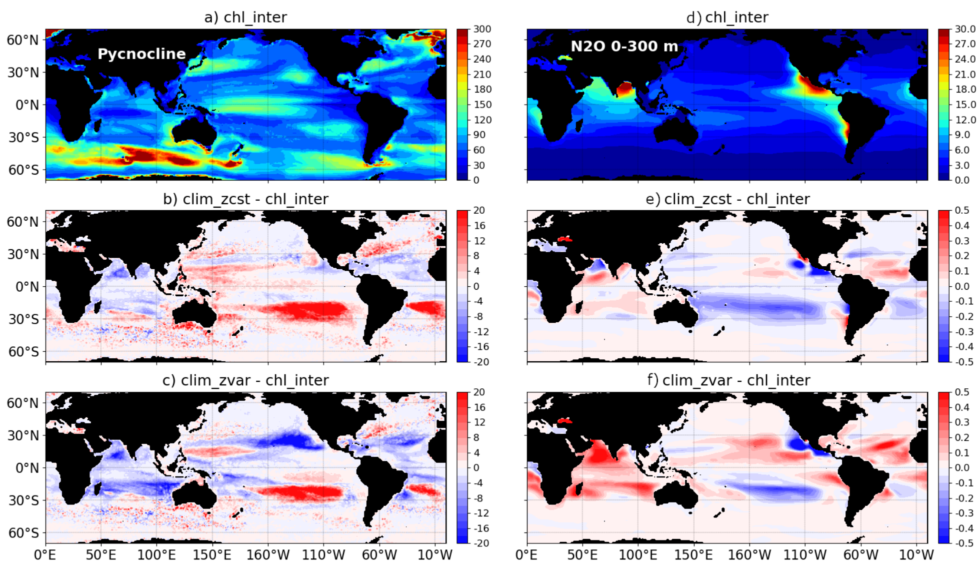

Figure 4: a-c) Depth of annual **pycnocline** (m) for 2009-2018, computed as the annual mean depth of the maximum of the Brunt-Väisälä frequency N^2(T, S) over the water column (Maes and O Kane, 2014). d-f) Mean **[N2O]** (micro-molN/m^3) over the first 300 meters depth for (upper line) chl_inter and its mean-state differences with (middle) clim_zcst and (bottom) clim_zvar.

https://doi.org/10.5194/esd-2022-28
Preprint. Discussion started: 22 August 2022

Earth System Dynamics
Discussions
Open Access

Anomalies of N2O concentration integrated over the first 300 meters of the water column (Figure 4, e and f) are in good agreement with patterns of pycnocline anomalies over the tropics (Figure 4, b and c). These comparable spatial structures attest that N2O anomalies are driven by perturbations of stratification in large parts of the tropical domain. Note that spatial patterns are robust against expanding the column used to perform the mean of N2O concentration up to 6000 meters, since most of the N2O perturbation is contained in the top 300 meters as reported also for physical variables.

In the South Pacific subtropical gyre, the concomitance of i) an increased temperature (Figure S2, c and d), ii) a reinforced transport (Figure *3*, b and c) and iii) a weakened stratification illustrated by a local deepening of the pycnocline (Figure 4, b and c), contributes to decrease the N2O concentration in both clim_zcst and clim_zvar (Figure 4, e and f). By contrast, in the South Indian Ocean and North tropical Atlantic the increase of N2O concentration seems to be mainly driven by the mean shoaling of the local pycnocline, as both regions exhibit contrasted perturbations in terms of transport and temperature. Finally, in the North-Pacific OMZ area, the strong N2O deficits in both clim_zcst and clim_zvar do not respond to stratification and transport anomalies but are rather driven by a local rise of O2 concentration (Figure S5). Considering an incomplete PLF contributes to overestimate the oxygen concentration in this OMZ and leads to a lack of local N2O production.

The relationship between N2O concentration and OHC300 in the Tropical Ocean is inferred next based on the three 20-years simulations (Figure *5*). Approaching the slope of the simulated distributions by a linear regression gives quite distinct tropical N2O production pathways along time as a function of the oceanic heat uptake: from 0.3 micro-molN m^{-2} per ZJ for the most simplified PLF scenario clim_zcst, to 1 micro-molN m^{-2} per ZJ for clim_zvar. The slope of the experiment with the higher level of realism in terms of interactivity (chl_inter) appears a solution between the two previous extremes, as it increases its N2O production by 0.8 micro-molN m^{-2} per ZJ. Each of these N2O production pathways will not forecast the same temporal evolution of the N2O budget and hence, the same climate in future. This result stresses the importance of having an interactive PLF in order to neither overestimate nor underestimate the N2O production forecast due to simplified representation of the PLF.

https://doi.org/10.5194/esd-2022-28
Preprint. Discussion started: 22 August 2022

Earth System Dynamics
Discussions
Open Access

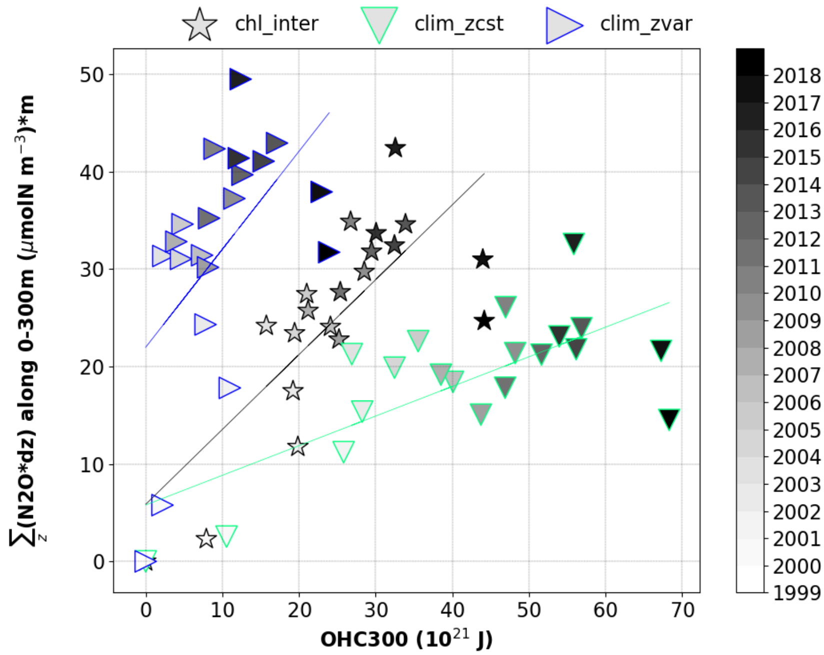

Figure 5: Annual N2O inventory over the first 300 meters depth (micro-molN/m^2/yr) as a function of the annual OHC300 (ZJ/yr) and annually averaged over an extended tropical domain (35°S-35°N).

d) Repercussions on oceanic N2O emissions

By perturbing the OHC, the ocean dynamics and the N2O production, the degree of realism of the PLF has non-negligible consequences on Dpn2o and thus on N2O emissions at the air-sea interface (Figure 6). Because the atmospheric partial pressure of N2O is identical among experiments, differences in Dpn2o are driven by differences in surface N2O concentration normalized by those in N2O solubility. It results that spatial patterns of Dpn2o anomalies (Figure 6) reflect differences in surface N2O concentration.

Interestingly, compared to a scenario considering a fully interactive PLF (chl_inter), an incomplete representation of the PLF underestimates Dpn2o in all OMZ regions of the northern hemisphere, which are strong emission zones (Figure 6, c and d). Large Dpn2o anomalies of -2.5 atm encompasses northern OMZ regions of the Indian, Pacific and Atlantic oceans and anomalies reach up to -5 natm locally. Consequently, clim_zcst and clim_zvar underestimate N2O fluxes by more than 12% in these OMZ regions compared to chl_inter. This result highlights that the way to represent the PLF can be an important source of uncertainty in modelling N2O fluxes. As a matter of fact, the oceanic contribution to the recent global N2O budget by Tian et al. (2020) is based on only five global ocean-biogeochemical models (as still only few models simulate marine N2O emissions). These models have different configurations of the PLF which adds considerable uncertainty to simulated marine N2O emissions.

https://doi.org/10.5194/esd-2022-28
Preprint. Discussion started: 22 August 2022

In subtropical gyres, the strong and direct effect of temperature (Figure S2, c and d) on [N2O] (Figure 4, e and f) is in line with Yang et al. (2020) who show that a solubility regime drives the seasonality of Dpn2o in that regions. Both clim_zcst and clim_zvar overestimate Dpn2o in subtropical gyres of the South Pacific and South Atlantic (Figure *6*, c and d). This leads to an overestimation of the regional N2O fluxes by 24% compared to a simulation having a complete and interactive PLF representation (chl_inter).

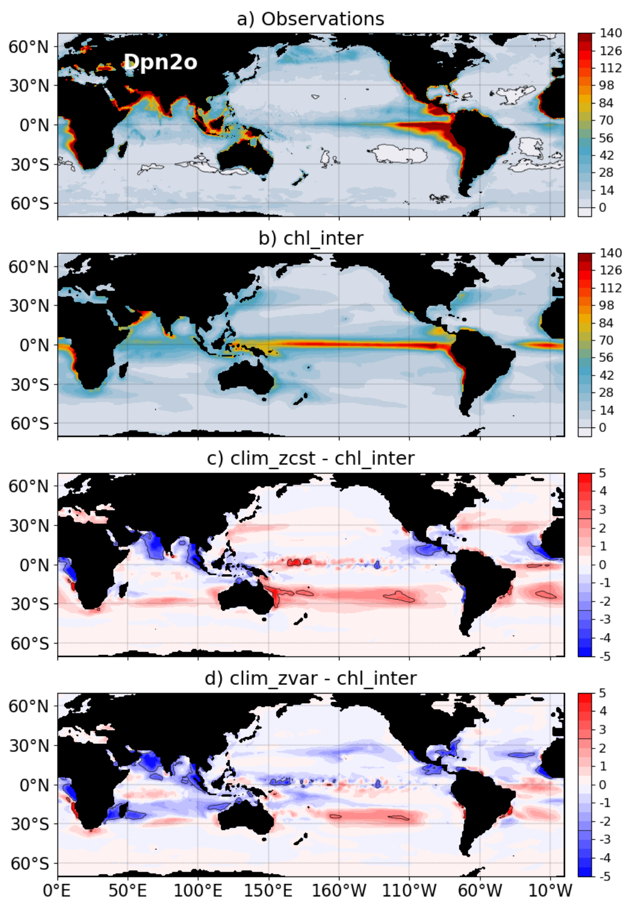

Figure 6: Mean sea-to-air **Dpn2o** (natm) computed from a) observations, b) chl_inter over the 2009-2018 period, and its differences with c) clim_zcst and d) clim_zvar compared to chl_inter.

4. Conclusion

In this study we use the ocean component (including ocean physics, sea ice and marine biogeochemistry) of a global Earth system model that contributed to the last CMIP project (CMIP6). Our ocean-biogeochemical model is one of the few currently able to represent an interactive phytoplankton-light feedback (PLF) by constraining the penetration of shortwave radiation into the ocean as a function of the chlorophyll concentration produced by the biogeochemical model. Three experiments have been run at the horizontal resolution currently used for intercomparisons of Earth system models (1°). Analyses are based on differences between a control run with an interactive PLF (chl_inter) and two experiments using an incomplete PLF (clim_zcst and clim_zvar) characterized by the use of a prescribed CHL climatology to interact with the incoming solar radiation. Changing the way to compute how the CHL filters the light penetration into the ocean reveals specific impacts of using an interactive PLF.

Our results show that the strategy used to account for the impact of the biology on light penetration significantly interfers with upper ocean heat uptake (Figure 1), and the associated dynamics (Figure *3*) and stratification in the tropics (Figure 4, a-c). Our set of forced ocean-biogeochemical experiments reveals that marine production of nitrous oxide (N2O) is sensitive to the representation of the PLF (Figure 4, d-f). The heat perturbations add to the uncertainty of modelled oceanic N2O production, and result in three N2O production trajectories with time (Figure *5*) that in turn trigger regional differences of Dpn2o and sea-air N2O fluxes (Figure 6). Compared to an ocean model using a fully interactive PLF (chl_inter), an incomplete PLF results in an overestimation of N2O fluxes by up to 24% in the south Pacific and south Atlantic subtropical gyres, and their reduction by up to 12% in OMZ of the northern hemisphere. Our results based on a model at CMIP6 state-of-the-art emphasize an overlooked important source of uncertainty in climate projections of marine N2O production and in current estimations of the marine nitrous oxide budget.

In subtropical gyres of the southern Hemisphere which are regions of low productivity, small CHL changes have a strong and direct effect on temperature (Figure S2, c and d), on transport (Figure *3*, b and c) and on the local stratification (Figure 4, b and c). These concomittant effects result in a local decrease of the N2O concentration in both experiments having a simplified PLF representation (clim_zcst and clim_zvar).

Our results also question the reliability of current modelled estimates of the area and volume of OMZ, as well as their trends in a future climate. The expansion rate of O2-depleted waters still remains unclear and its controlling mechanisms are not yet fully understood (and represented in today's models). Observations assessed that oceans have already lost around 2% of the global marine oxygen since 1960 (Schmidtko et al., 2017). The expansion of OMZ is expected to result in an increase of the volume of water suitable for denitrification and to have an impact on the production and decomposition of N2O (Freing et al., 2012). Our set of experiments highlights that an incomplete representation of the PLF underestimates the expansion of oxygen-depleted waters over the 20 years of simulation in comparison to chl_inter. In clim_zcst and clim_zvar the global volume (0-1000 m) of hypoxic water with [O2] under 50 mmol m^{-3} is up to 2.3 10^{14} m^3 lower in 2018 compared to that of the control run chl_inter. Thus an incomplete representation of the PLF might lead to an underestimation by 1.2 % of the modelled tropical volume of low-oxygenated waters after 20 years.

Recent regional studies demonstrated that the interactive PLF strongly affects upwelling systems of the south Pacific and Atlantic oceans (Hernandez et al., 2017; Echevin et al., 2021). Coastal upwellings are known to be a place of high N2O production, with an annual N2O flux totting up 20% of the global fluxes while these systems occupy less than 3% of the ocean area (Yang et al., 2020). However, in our results main modelled perturbations are rather localized over OMZ or subtropical gyres (Figure 4; Figure *6*). While the latter regional studies have been performed using horizontal resolutions suitable to represent the complex dynamics of coastal upwellings (from 10 km to about 28 km), it is well-established that climate models resolution (~1-degree of horizontal resolution) does not allow to resolve these dynamics. The present framework was designed to evaluate the sensitivity of CMIP models to the representation of the PLF so why it used the spatial horizontal resolution of CMIP-like experiments. A step further would be to evaluate how this sensitivity depends on the horizontal resolution by running experiments at higher resolution with the same climate model. This would help to better determine how the resolution of coastal upwelling systems may impact the modelled N2O inventory through different PLF representations, as well as the associated modelled range of uncertainty.

Code availability

Sources for NEMO and PISCES codes are available from https://forge.nemo-ocean.eu/nemo.

Acknowledgements

The OHC data were collected and made freely available by the International Argo Program and the national programs that contribute to it (https://argo.ucsd.edu, https://www.ocean-ops.org). The Argo Program is part of the Global Ocean Observing System. R. Séférian acknowledges the European Union's Horizon 2020 research and innovation program under grant agreement No. 101003536 (ESM2025 – Earth System Models for the Future).

References

Anderson,W. G., Gnanadesikan, A., Hallberg, R., Dunne, J., and Samuels, B. L.: Impact of ocean color on the maintenance of the Pacific Cold Tongue, Geophys. Res. Lett., 34, L11609, doi:10.1029/2007GL030100, 2007.

Aumont, O., Ethé, C., Tagliabue, A., Bopp, L., and Gehlen, M.: PISCES-v2: An ocean biogeochemical model for carbon and ecosystem studies. Geoscientific Model Development, 8, 2465–2513, 2015.

Arévalo-Martinez, D. L., Kock, A., Steinhoff, T., Brandt, P., Dengler, M., Fischer, T., Körtzinger, A., and Bange, H. W.: Nitrous oxide during the onset of the Atlantic cold tongue, J. Geophys. Res. Oceans, 122, 171–184, doi:10.1002/2016JC012238, 2017.

Arévalo-Martínez, D. L., Steinhoff, T., Brandt, P., Körtzinger, A., Lamont, T., Rehder, G., and Bange, H. W.: N2O emissions from the northern Benguela upwelling system. Geophysical Research Letters, 46, 3317–3326. https://doi.org/10.1029/2018GL081648, 2019.

Berthet, S., Séférian, R., Bricaud, C., Chevallier, M., Voldoire, A., and Ethé, C.: Evaluation of an online grid-coarsening algorithm in a global eddy-admitting ocean biogeochemical model. Journal of Advances in Modeling Earth Systems, 11, 1759–1783. https://doi.org/10.1029/2019MS001644, 2019.

Bopp, L., Resplandy, L., Orr, J. C., Doney, S. C., Dunne, J. P., Gehlen, M., Halloran, P., Heinze, C., Ilyina, T., Séférian, R., Tjiputra, J., and Vichi, M.: Multiple stressors of ocean ecosystems in the 21st century: projections with CMIP5 models, Biogeosciences, 10, 6225–6245, doi:10.5194/bg-10-6225-2013, 2013.

https://doi.org/10.5194/esd-2022-28
Preprint. Discussion started: 22 August 2022

Cheng, L., Trenberth, K. E., Palmer, M. D., Zhu, J., and Abraham, J. P.: Observed and simulated full-depth ocean heat-content changes for 1970–2005, Ocean Sci., 12, 925–935, https://doi.org/10.5194/os-12-925-2016, 2016.

Cocco, V., Joos, F., Steinacher, M., Frölicher, T. L., Bopp, L., Dunne, J., Gehlen, M., Heinze, C., Orr, J., Oschlies, A., Schneider, B., Segschneider, J., and Tjiputra, J.: Oxygen and indicators of stress for marine life in multi-model global warming projections, Biogeosciences, 10, 1849–1868, doi:10.5194/bg-10-1849-2013, 2013.

Echevin, V., Hauschildt, J., Colas, F., Thomsen, S., and Aumont, O.: Impact of chlorophyll shading on the Peruvian upwelling system. Geophysical Research Letters, 48, e2021GL094429. https://doi.org/10.1029/2021GL094429, 2021.

Freing, A., Wallace, D. W. R., and Bange, H. W.: Global oceanic production of nitrous oxide. Philos. Trans. R. Soc. London Ser. B, **367**, 1245–1255, 2012.

Garcia, H. E., Locarnini, R. A., Boyer, T. P., Antonov, J. I., Baranova, O.K., Zweng, M. M., Reagan, J. R., and Johnson, D. R.: World Ocean Atlas 2013, Volume 3: Dissolved Oxygen, Apparent Oxygen Utilization, and Oxygen Saturation. S. Levitus, Ed., A. Mishonov Technical Ed.; NOAA Atlas NESDIS 75, 27 pp, 2014.

Gildor, H., and Naik, N. H.: Evaluating the effect of interannual variations of surface chlorophyll on upper ocean temperature, J. Geophys. Res., 110, C07012, doi:10.1029/2004JC002779, 2005.

Gnanadesikan, A., and Anderson, W. G.: Ocean water clarity and the ocean general circulation in a coupled climate model, J. Phys. Ocean., 39, 314–332, 2009.

Good, S. A., Martin, M. J., and Rayner, N. A.: EN4: quality controlled ocean temperature and salinity profiles and monthly objective analyses with uncertainty estimates, Journal of Geophysical Research: Oceans, doi:10.1002/2013JC009067, 2013.

Hajima, T., Watanabe, M., Yamamoto, A., Tatebe, H., Noguchi, M. A., Abe, M., Ohgaito, R., Ito, A., Yamazaki, D., Okajima, H., Ito, A., Takata, K., Ogochi, K., Watanabe, S., and Kawamiya, M.: Development of the MIROC-ES2L Earth system model and the evaluation of biogeochemical processes and feedbacks, Geosci. Model Dev., 13, 2197–2244, https://doi.org/10.5194/gmd-13-2197-2020, 2020.

Heinze, C., Blenckner, T., Martins, H., Rusiecka, D., Döscher, R., Gehlen, M., Gruber, N., Holland, E., Hov, Ø. Joos, F., Matthews, J. B. R., Rødven, R., and Wilson, S. : The quiet crossing of ocean tipping points, Proceedings of the National Academy of Sciences, 118 (9) e2008478118; DOI: 10.1073/pnas.2008478118, 2021.

Hernandez, O., Jouanno, J., Echevin, V., and Aumont, O.: Modification of sea surface temperature by chlorophyll concentration in the Atlantic upwelling systems, J. Geophys. Res. Oceans, 122, 5367–5389, doi:10.1002/2016JC012330, 2017.

Hutchins, D.A., and Capone, D.G: The marine nitrogen cycle: new developments and global change. Nat. Rev. Microbiol., https://doi-org.insu.bib.cnrs.fr/10.1038/s41579-022-00687-z, 2022.

Ilyina, T., Six, K. D., Segschneider, J., Maier-Reimer, E., Li, H., and Núñez-Riboni, I.: Global ocean biogeochemistrymodel HAMOCC: Model architecture and performance as component of the MPI-Earth system model in different CMIP5 experimental realizations,J.Adv.Model.EarthSyst.,5, 287–315, doi:10.1029/2012MS000178, 2013.

https://doi.org/10.5194/esd-2022-28
Preprint. Discussion started: 22 August 2022

Earth System Dynamics
Discussions

IPCC: Summary for Policymakers, in: IPCC Special Report on the Ocean and Cryosphere in a Changing Climate, edited by: Pörtner,H.-O., Roberts, D.C., Masson-Delmotte, V., Zhai, P., Tignor, M., Poloczanska, E., Mintenbeck, K., Nicolai, M., Okem, A., Petzold, J., Rama, B., and Weyer, N., 2019.

Ji, Q., Babbin, A. R., Jayakumar, A., Oleynik, S., and Ward, B. B.: Nitrous oxide production by nitrification and denitrification in the Eastern Tropical South Pacific oxygen minimum zone, Geophys. Res. Lett., 42, 10,755–10,764, doi:10.1002/2015GL066853, 2015.

Ji, Q., Buitenhuis, E., Suntharalingam, P., Sarmiento, J. L., and Ward, B. B.: Global nitrous oxide production determined by oxygen sensitivity of nitrification and denitrification. Global Biogeochemical Cycles, 32, 1790–1802. https://doi.org/10.1029/2018GB005887, 2018.

Kahru, M., Leppaenen, J.-M., and Rud, O.: Cyanobacterial blooms cause heating of the sea surface, Mar. Ecol.-Prog. Ser., 101, 1–7, 1993.

Kolodziejczyk, N., Llovel, W., and Portela, E.: Interannual variability of upper ocean water masses as inferred from Argo Array, Journal of Geophysical Research: Oceans. doi:10.1029/2018JC014866, 2019.

Kolodziejczyk, N., Prigent-Mazella, A., and Gaillard, F.: ISAS temperature and salinity gridded fields. SEANOE. https://doi.org/10.17882/52367, 2021.

Kortzinger, A., Hedges, J. I., and Quay, P. D.: Redfield ratios revisited: removing the biasing effect of anthropogenic CO2, Limnol. Oceanogr., 46, 964–970, 2001.

Kwiatkowski, L., Torres, O., Bopp, L., Aumont, O., Chamberlain, M., Christian, J. R., Dunne, J. P., Gehlen, M., Ilyina, T., John, J. G., Lenton, A., Li, H., Lovenduski, N. S., Orr, J. C., Palmieri, J., Santana-Falcón, Y., Schwinger, J., Séférian, R., Stock, C. A., Tagliabue, A., Takano, Y., Tjiputra, J., Toyama, K., Tsujino, H., Watanabe, M., Yamamoto, A., Yool, A., and Ziehn, T.: Twenty-first century ocean warming, acidification, deoxygenation, and upper-ocean nutrient and primary production decline from CMIP6 model projections, Biogeosciences, 17, 3439–3470, https://doi.org/10.5194/bg-17-3439-2020, 2020.

Lam, P., and Kuypers, M.: Microbial Nitrogen Cycling Processes in Oxygen Minimum Zones, Annual Review of Marine Science 3:1, 317-345, doi:10.1146/annurev-marine-120709-142814, 2011.

Lengaigne, M., Madec, G., Bopp, L., Menkes,C., Aumont, O., and Cadule, P.: Bio-physical feedbacks in the Arctic Ocean using an Earth system model, Geophys. Res. Lett., 36, L21602, doi:10.1029/2009GL040145, 2009.

Lengaigne, M., Menkes, C., Aumont, O., et al.: Influence of the oceanic biology on the tropical Pacific climate in a coupled general circulation model. Clim Dyn **28,** 503–516, https://doi.org/10.1007/s00382-006-0200-2, 2007.

Levitus, S., Antonov, J. I., Boyer, T. P., Baranova, O. K., Garcia, H. E., Locarnini, R. A., Mishonov, A. V., Reagan, J. R., Seidov, D., Yarosh, E. S., and Zweng, M. M.: World Ocean heat content and thermosteric sea level change (0-2000 m) 1955-2010. Geophys. Res. Lett. , 39, L10603, doi:10.1029/2012GL051106, 2012.

Liang, X., Liu, C. R., Ponte, M., and Chambers, D. P.: A Comparison of the Variability and Changes in Global Ocean Heat Content from Multiple Objective Analysis Products During the Argo Period, J. Climate, 34(19), 7875–7895, https://doi.org/10.1175/JCLID-20-0794.1, 2021.

Llovel, W., and Terray, L.: Observed southern upper-ocean warming over 2005–2014 and associated mechanisms, Environ. Res. Lett., 11, 124023, 2016.

Llovel, W., Kolodziejczyk, N., Close, S., Penduff, T., Molines, J.-M., and Terray, L.: Imprint of intrinsic ocean variability on decadal trends of regional sea level and ocean heat content using synthetic profiles, Environ. Res. Lett., 17, 044063, 2022.

Locarnini, R. A., Mishonov, A. V., Antonov, J. I., Boyer, T. P., Garcia, H. E., Baranova, O. K., Zweng, M. M., Paver, C. R., Reagan, J. R., Johnson, D. R., Hamilton, M., and Seidov, D.: World Ocean Atlas 2013, Volume 1: Temperature. S. Levitus, Ed., A. Mishonov Technical Ed.; NOAA Atlas NESDIS 73, 40 pp, 2013.

Löptien, U., Eden, C., Timmermann, A., and Dietze, H.: Effects of biologically induced differential heating in an eddy-permitting coupled ocean-ecosystem model, J. Geophys. Res., 114, C06011, doi:10.1029/2008JC004936, 2009.

Lyman, J., Good, S., Gouretski, V. et al.: Robust warming of the global upper ocean. Nature **465,** 334–337, https://doi.org/10.1038/nature09043, 2010.

Madec, G.: Nemo ocean engine. Note du Pôle de modélisation de l'Institut Pierre-Simon Laplace, 27, 1–217, 2008.

Maes, C., and O'Kane, T. J.: Seasonal variations of the upper ocean salinity stratification in the Tropics, J. Geophys. Res. Oceans, 119, 1706–1722, doi:10.1002/2013JC009366, 2014.

Manizza, M., Le Quéré, C., Watson, A. J., and Buitenhuis, E. T.: Bio-optical feedbacks among phytoplankton, upper ocean physics and sea-ice in a global model, Geophys. Res. Lett., 32, L05603, doi:10.1029/2004GL020778, 2005.

Manizza, M., Le Quéré, C., Watson, A. J., and Buitenhuis, E. T.: Ocean biogeochemical response to phytoplankton-light feedback in a global model, J. Geophys. Res., 113, C10010, doi:10.1029/2007JC004478, 2008.

Martinez-Rey, J., Bopp, L., Gehlen, M., Tagliabue, A., and Gruber, N.: Projections of oceanic N_2O emissions in the 21st century using the IPSL Earth system model, Biogeosciences, 12, 4133–4148, https://doi.org/10.5194/bg-12-4133-2015, 2015.

Marzeion, B., Timmermann, A., Murtugudde, R., and Jin, F.: Biophysical Feedbacks in the Tropical Pacific, Journal of Climate, 18(1), 58-70, 2005.

Meyssignac, B, Boyer, T, Zhao, Z, Hakuba, MZ, Landerer, FW, Stammer, D, Köhl, A, Kato, S, L'Ecuyer, T, Ablain, M, Abraham, JP, Blazquez, A, Cazenave, A, Church, JA, Cowley, R, Cheng, L, Domingues, CM, Giglio, D, Gouretski, V, Ishii, M, Johnson, GC, Killick, RE, Legler, D, Llovel, W, Lyman, J, Palmer, MD, Piotrowicz, S, Purkey, SG, Roemmich, D, Roca, R, Savita, A, von Schuckmann, K, Speich, S, Stephens, G, Wang, G, Wijffels, SE, and Zilberman, N: Measuring Global Ocean Heat Content to Estimate the Earth Energy Imbalance. Front. Mar. Sci. 6:432. doi: 10.3389/fmars.2019.00432, 2019.

Mignot, J., Swingedouw, D., Deshayes, J., Marti, O., Talandier, C., Séférian, R., Lengaigne, M., and Madec, G.: On the evolution of the oceanic component of the IPSL climate models from CMIP3 to CMIP5: A mean state comparison, Ocean Modelling, Volume 72, Pages 167-184, ISSN 1463-5003, https://doi.org/10.1016/j.ocemod.2013.09.001, 2013.

Morel, A.: Optical modeling of the upper ocean in relation to its biogenous matter content (Case I waters). J Geophys Res 93:10749–10768, 1988.

Morel, A., and Berthon, J.-F.: Surface pigments, algal biomass profiles, and potential production of the euphotic layer : Relationships reinvestigated in view of remote-sensing applications. Limnol. Oceanogr., 34(8), 1545–1562, 1989.

Morel, A., and Maritorena, S.: Bio-optical properties of oceanic waters: a reappraisal. J Geophys Res 106:7163–7180, 2001.

Murtugudde, R., Beauchamp, J., McClain, C. R., Lewis, M., and Busalacchi, A. J.: Effects of Penetrative Radiation on the Upper Tropical Ocean Circulation, Journal of Climate, 15(5), 470-486, 2002.

Myhre, G., Shindell, D., Bréon, F.-M., Collins, W., Fuglestvedt, J., Huang, J., Koch, D., Lamarque, J.-F., Lee, D., Mendoza, B., Nakajima, T., Robock, A., Stephens, G., Takemura, T., and Zhang, H.: Anthropogenic and Natural Radiative Forcing. In: Climate Change 2013: The Physical Science Basis. Contribution of Working Group I to the Fifth Assessment Report of the Intergovernmental Panel on Climate Change [Stocker, T.F., D. Qin, G.-K. Plattner, M. Tignor, S.K. Allen, J. Boschung, A. Nauels, Y. Xia, V. Bex and P.M. Midgley (eds.)]. Cambridge University Press, Cambridge, United Kingdom and New York, NY, USA, 2013.

Nakamoto, S., Kumar, S. P., Oberhuber, J. M., Ishizaka, J., Muneyama, K., and Frouin, R.: Response of the equatorial Pacific to chlorophyll pigment in a mixed layer isopycnical ocean general circulation model, Geophys. Res. Lett., 28, 2021– 2024, 2001.

Oschlies, A.: Feedbacks of biotically induced radiative heating on upper-ocean heat budget, circulation, and biological production in a coupled ecosystem-circulation model, J. Geophys. Res., 109, C12031, doi:10.1029/2004JC002430, 2004.

Park, JY., Kug, JS., Seo, H. et al.: Impact of bio-physical feedbacks on the tropical climate in coupled and uncoupled GCMs. Clim Dyn **43,** 1811–1827, https://doi.org/10.1007/s00382-013-2009-0, 2014.

Patara, L., Vichi, M., Masina, S. et al.: Global response to solar radiation absorbed by phytoplankton in a coupled climate model. Clim Dyn **39,** 1951–1968, https://doi.org/10.1007/s00382-012-1300-9, 2012.

Ravishankara, A. R., J. S. Daniel, and R. W. Portmann, 2009: Nitrous oxide (N2O): The dominant ozone-depleting substance emitted in the 21st century. Science, **326**, 123–125, 2009.

Roemmich, D., and Gilson, J.: The 2004–2008 mean and annual cycle of temperature, salinity, and steric height in the global ocean from the Argo Program. Prog. Oceanogr., 82, 81–100, https://doi.org/10.1016/j.pocean.2009.03.004, 2009.

Sallée, JB., Pellichero, V., Akhoudas, C. et al.: Summertime increases in upper-ocean stratification and mixed-layer depth. Nature 591**,** 592–598, https://doi.org/10.1038/s41586-021-03303-x, 2021.

Schmidtko, S., Stramma, L., and Visbeck, M.: Decline in global oceanic oxygen content during the past five decades. Nature 542, 335–339, 2017.

Séférian, R., Berthet, S., Yool, A. et al.: Tracking Improvement in Simulated Marine Biogeochemistry Between CMIP5 and CMIP6. Curr Clim Change Rep **6,** 95–119, https://doi.org/10.1007/s40641-020-00160-0, 2020.

Séférian, R., Nabat, P., Michou, M., Saint-Martin, D., Voldoire, A., Colin, J., et al.: Evaluation of CNRM Earth-System model, CNRM-ESM2-1: role of Earth system processes in present-day and future climate. Journal of Advances in Modeling Earth Systems, 11. https://doi.org/10.1029/2019MS001791, 2019.

Sweeney, C., Gnanadesikan, A., Griffies, S. M., Harrison, M. J., Rosati, A. J., and Samuels, B. L.: Impacts of Shortwave Penetration Depth on Large-Scale Ocean Circulation and Heat Transport, Journal of Physical Oceanography, 35(6), 1103-1119, 2005.

https://doi.org/10.5194/esd-2022-28
Preprint. Discussion started: 22 August 2022

Takahashi, T., Broecker, W. S., and Langer, S.: Redfield ratio based on chemical data from isopycnal surfaces, J. Geophys. Res., 90, 6907–6924, 1985.

Tian, H., Xu, R., Canadell, J.G., R. L. Thompson, W. Winiwarter, P. Suntharalingam, E. A. Davidson, P. Ciais, R. B. Jackson, G. Janssens-Maenhout, M. J. Prather, P. Regnier, N. Pan, S. Pan, G. Peters, H. Shi, F. N. Tubiello, S. Zaehle, F. Zhou, A. Arneth, G. Battaglia, S. Berthet, L. Bopp, A. F. Bouwman, E. T. Buitenhuis, J. Chang, Martyn P. Chipperfield, S. R.S. Dangal, E. Dlugokencky, J. Elkins, Bradley D. Eyre, B. Fu, B. Hall, A. Ito, F. Joos, P. B. Krummel, A. Landolfi, G. G. Laruelle, R. Lauerwald, W. Li, S. Lienert, T. Maavara, M. MacLeod, D. B. Millet, S. Olin, P. K. Patra, R. G. Prinn, P. A. Raymond, D. J. Ruiz, Guido R. van der Werf, N. Vuichard, J. Wang, R. Weiss, K. C. Wells, C. Wilson, J. Yang and Y. Yao: A comprehensive quantification of global nitrous oxide sources and sinks. Nature 586, 248–256, https://doi.org/10.1038/s41586-020-2780-0, 2020.

Tiano, L., Garcia-Robledo, E., Dalsgaard, T., Devol, A. H., Ward, B. B., Ulloa, O., Canfield, D. E., and Revsbech, N. P.: Oxygen distribution and aerobic respiration in the north and south eastern tropical Pacific oxygen minimum zones. Deep Sea Research Part I: Oceanographic Research Papers, Volume 94, Pages 173-183, https://doi.org/10.1016/j.dsr.2014.10.001, 2014.

Timmermann, A., and Jin, F.-F.: Phytoplankton influences on tropical climate, Geophys. Res. Lett., 29(23), 2104, doi:10.1029/2002GL015434, 2002.

Tsujino, H., Urakawa, S., Nakano, H., Small, R. J., Kim, W. M., Yeager, S. G., Danabasoglu, G., Suzuki, T., Bamber J. L., Bentsen, M., Böning, C. W., Bozec, A., Chassignet, E. P., Curchitser, E., Boeira Dias, F., Durack, P. J., Griffies, S. M., Harada, Y., Ilicak, M., Josey, S. A., Kobayashi, C., Kobayashi, S., Komuro, Y., Large, W. G., Le Sommer, J., Marsland, S. J., Masina, S., Scheinert, M., Tomita, H., Valdivieso, M., and Yamazaki, D.: JRA-55 based surface dataset for driving ocean–sea-ice models (JRA55-do), Ocean Model., 130, 79–139, https://doi.org/10.1016/j.ocemod.2018.07.002, 2018.

Tsujino, H., Urakawa, L. S., Griffies, S. M., Danabasoglu, G., Adcroft, A. J., Amaral, A. E., Arsouze, T., Bentsen, M., Bernardello, R., Böning, C. W., Bozec, A., Chassignet, E. P., Danilov, S., Dussin, R., Exarchou, E., Fogli, P. G., Fox-Kemper, B., Guo, C., Ilicak, M., Iovino, D., Kim, W. M., Koldunov, N., Lapin, V., Li, Y., Lin, P., Lindsay, K., Liu, H., Long, M. C., Komuro, Y., Marsland, S. J., Masina, S., Nummelin, A., Rieck, J. K., Ruprich-Robert, Y., Scheinert, M., Sicardi, V., Sidorenko, D., Suzuki, T., Tatebe, H., Wang, Q., Yeager, S. G., and Yu, Z.: Evaluation of global ocean–sea-ice model simulations based on the experimental protocols of the Ocean Model Intercomparison Project phase 2 (OMIP-2), Geosci. Model Dev., 13, 3643–3708, https://doi.org/10.5194/gmd-13-3643-2020, 2020.

Wanninkhof, R.: Relationship between wind speed and gas exchange over the ocean, J. Geophys. Res., 97, 7373–7382, doi:10.1029/92JC00188, 1992.

Wanninkhof, R.: Relationship between wind speed and gas exchange over the ocean revisited, Limnol. Oceanogr. Methods, 12, doi:10.4319/lom.2014.12.351, 2014.

Yang, S., Chang, B. X., Warner, M. J., Weber, T. S., Bourbonnais, A. M., Santoro, A. E., Kock, A., Sonnerup, R. E., Bullister, J. L., Wilson, S. T., and Bianchi, D. : Global reconstruction reduces the uncertainty of oceanic nitrous oxide emissions and reveals a vigorous seasonal cycle, Proceedings of the National Academy of Sciences, 117 (22) 11954-11960; DOI: 10.1073/pnas.1921914117, 2020.

Valente, A, Sathyendranath, S, Brotas, V, Groom, S, Grant, M, Taberner, M, Antoine, D, Arnone, R, Balch, W, Barker, K, Barlow, R, Bélanger, S, Berthon, JF, Besiktepe, S, Brando, V, Canuti, E, Chavez, F, Claustre, H, Crout, R, Frouin, R, Garcìa-Soto, C, Gibb, SW, Gould, R, Hooker, S, Kahru, M, Klein, H, Kratzer, S, Loisel, H, McKee, D, Mitchell, BG, Moisan, T, Muller-Karger, F., O'Dowd, L, Ondrusek, M, Poulton, A, Repecaud, M, Smyth, T, Sosik, HM, Twardowski, M, Voss, K, Werdell, J, Wernand, M, and Zibordi, G: A compilation of global bio-optical in situ data for ocean-colour satellite applications. Earth Syst. Sci. Data, 8, 235–252, doi: 10.5194/essd-8-235-2016, 2016.

Weiss, R. F., and Price, B. A.: Nitrous oxide solubility in water and seawater Marine Chemistry, Volume 8, Issue 4, Pages 347-359; DOI: 10.1016/0304-4203(80)90024-9, 1980.

Wilson, S. T., Al-Haj, A. N., Bourbonnais, A., Frey, C., Fulweiler, R. W., Kessler, J. D., Marchant, H. K., Milucka, J., Ray, N. E., Suntharalingam, P., Thornton, B. F., Upstill-Goddard, R. C., Weber, T. S., Arévalo-Martínez, D. L., Bange, H. W., Benway, H. M., Bianchi, D., Borges, A. V., Chang, B. X., Crill, P. M., del Valle, D. A., Farías, L., Joye, S. B., Kock, A., Labidi, J., Manning, C. C., Pohlman, J. W., Rehder, G., Sparrow, K. J., Tortell, P. D., Treude, T., Valentine, D. L., Ward, B. B., Yang, S., and Yurganov, L. N.: Ideas and perspectives: A strategic assessment of methane and nitrous oxide measurements in the marine environment, Biogeosciences, 17, 5809–5828, https://doi.org/10.5194/bg-17-5809-2020, 2020.